Mon. Not. R. Astron. Soc. **347,** 1173–1179 (2004)

ULTRACAM photometry of the eclipsing cataclysmic variable OU Vir

W. J. Feline,[1⋆] V. S. Dhillon,[1] T. R. Marsh,[2,3] M. J. Stevenson,[1] C. A. Watson[1] and C. S. Brinkworth[3]

[1]*Department of Physics and Astronomy, University of Sheffield, Sheffield, S3 7RH*
[2]*Department of Physics, University of Warwick, Coventry CV4 7AL*
[3]*Department of Physics and Astronomy, University of Southampton, Southampton, SO17 1BJ*

Accepted 2003 October 13. Received 2003 October 10; in original form 2003 August 7

ABSTRACT

We present high-speed, three-colour photometry of the faint eclipsing cataclysmic variable OU Vir. For the first time in OU Vir, separate eclipses of the white dwarf and the bright spot have been observed. We use timings of these eclipses to derive a purely photometric model of the system, obtaining a mass ratio of $q = 0.175 \pm 0.025$, an inclination of $i = 79\overset{\circ}{.}2 \pm 0\overset{\circ}{.}7$ and a disc radius of $R_{\rm d}/a = 0.2315 \pm 0.0150$. We separate the white dwarf eclipse from the light curve and, by fitting a blackbody spectrum to its flux in each passband, obtain a white dwarf temperature of $T = 13\,900 \pm 600$ K and a distance of $D = 51 \pm 17$ pc. Assuming that the primary obeys the Nauenberg mass–radius relation for white dwarfs and allowing for temperature effects, we also find a primary mass $M_{\rm w}/{\rm M}_{\odot} = 0.89 \pm 0.20$, a primary radius $R_{\rm w}/R_{\odot} = 0.0097 \pm 0.0031$ and an orbital separation $a/R_{\odot} = 0.74 \pm 0.05$.

Key words: binaries: close – binaries: eclipsing – stars: dwarf novae – stars: individual: OU Vir – novae, cataclysmic variables.

1 INTRODUCTION

Cataclysmic variable stars (CVs) are short-period binary systems which typically consist of a cool main-sequence star transferring mass via a gas stream and an accretion disc to a white dwarf primary. The impact of the stream with the accretion disc forms a so-called 'bright spot', which, in systems that are significantly inclined to our line of sight, can cause a rise in the observed flux as this region rotates into view, resulting in an 'orbital hump' in the light curve. In high-inclination systems, eclipses of the white dwarf, the bright spot and the disc by the red dwarf secondary can also occur. Analysis of these eclipses can yield determinations of system parameters such as the mass ratio q, the orbital inclination i and the radius of the accretion disc $R_{\rm d}$ (e.g. Wood et al. 1989). Eclipsing systems are therefore valuable sources of data on CVs.

Dwarf novae are a subtype of CVs which show intermittent luminosity increases of 2–5 mag, known as outbursts. A further subtype of dwarf novae are the SU UMa stars, which exhibit superoutbursts at regular intervals, during which the luminosity increases by ∼0.7 mag over the normal outburst maximum. These superoutbursts are characterized by the presence of superhumps – increases in brightness that usually recur at a slightly longer period than the orbital cycle. There is found to be a relationship between this superhump period excess ϵ and the mass ratio (Patterson 1998). Determinations of the mass ratios of SU UMa stars are therefore useful to calibrate this relation, which can then be used to determine the mass ratios of other SU UMa stars.

OU Vir is a faint ($V \sim 18$; Mason et al. 2002) eclipsing CV with a period of 1.75 hr which has been seen in outburst and probably superoutburst (Vanmunster, Velthuis & McCormick 2000), marking it as an SU UMa dwarf nova. Mason et al. (2002) presented time-resolved, multicolour photometry and spectroscopy of OU Vir, concluding that the eclipse is of the bright spot and the disc, but not of the white dwarf. In this paper, we present light curves of OU Vir, obtained with ULTRACAM, an ultra-fast, triple-beam CCD camera; for more details, see Dhillon & Marsh (2001); Dhillon et al. (in preparation).

2 OBSERVATIONS

OU Vir was observed on the nights of 2002 May 16 and 2003 May 19, 20, 22 and 25 using ULTRACAM on the 4.2-m William Herschel Telescope (WHT) at the Isaac Newton Group of Telecopes, La Palma. The observations were obtained simultaneously in the r', g' and u' colour bands on 2002 May 16, the z', g' and u' bands on 2003 May 19, and the i', g' and u' bands on subsequent nights. Data reduction was carried out using the ULTRACAM pipeline data reduction software. Unfortunately, we were unable to observe a standard star in the z' band using ULTRACAM, so the zero-point for this filter was chosen to be the same as for the i' band; this will only affect the scale of the z' light curve, not its shape. All the data were corrected to zero airmass using the nightly extinction coefficients measured by the Carlsberg Meridian Telescope on La Palma in the r' filter,

⋆E-mail: w.feline@shef.ac.uk

and converted to other colour bands using the procedure described by King (1985) and the effective wavelengths of the filters given by Fukugita et al. (1996).

The light curves of OU Vir are shown in Fig. 1. On 2002 May 16, the exposure time was 0.5 s and the data points were separated by approximately 4.9 s. These data were obtained on the first night of commissioning and hence were adversely affected by typical commissioning problems – chiefly, excess noise in the u' band and limited time resolution owing to the dead-time between exposures. The data taken in 2003 had no such problems, and hence the dead-time was reduced to 0.025 s. The exposure times for these observations varied according to the seeing on the night, and were 9.2 s on 2003 May 19, 5.2 s on 2003 May 20 and 4.2 s thereafter.

3 LIGHT-CURVE MORPHOLOGY

OU Vir was observed during descent from superoutburst in both 2002 and 2003. Mason et al. (2002) found that for OU Vir out of eclipse and during quiescence, $V = 18.08$ and $B - V = 0.14$, which corresponds to $g' \sim 0.2$ mJy (Smith et al. 2002). Vanmunster et al. (2000) quote an outburst amplitude of approximately 4 mag (corresponding to a peak g' flux of ∼8.4 mJy). The system appears to be significantly below superoutburst maximum on 2002 May 16, and almost at its quiescent brightness during the 2003 observations: the maximum superoutburst flux we have observed is ∼1.2 mJy on 2002 May 16, and the out-of-eclipse quiescent flux is ∼0.2 mJy on 2003 May 22 and 25.

As the descent from superoutburst is typically much slower than the ascent, we suspect that the 2002 observations took place during the former state, but of course we cannot be certain. The 2002 data are, as far as we are aware, the only observations of this superoutburst. The 2003 superoutburst was first reported on May 2 (Kato 2003). The superhump is visible in both the 2002 May 16 light curve at phase ∼−0.45 and the 2003 May 20 light curve at phase ∼−0.2, but is not visible in later data, either because it had faded or because it was at a phase which was not observed.

The lower three panels of Fig. 1 show changes in the eclipse morphology that occur during the descent from superoutburst. Importantly, the eclipse morphology changed drastically from a single sharp ingress and egress on 2003 May 20 to separate eclipses of the white dwarf and the bright spot in the u' and g' bands on 2003 May 25. The bright-spot ingress is also visible in the g' data of 2003 May 22. (The second egress feature visible in this light curve is more gradual than it appears in the compressed scale of Fig. 1, and is mainly caused by the egress of the disc.) This evolution of the eclipse morphology is typical for a system going from (super)outburst to quiescence (see, for example, Rutten et al. 1992).

4 ECLIPSE CONTACT PHASES

The white dwarf eclipse contact phases given in Tables 1 and 2 were determined using the techniques described by Wood, Irwin & Pringle (1985), Wood et al. (1986) and Wood et al. (1989). A median filter was used to smooth the data, the derivative of which was then calculated numerically. A box-car filter was applied to this derivative, and simple searches were made to locate the minimum and maximum values of the derivative corresponding to the mid-points of ingress ϕ_i and egress ϕ_e. (In fact, this method locates the steepest part of the ingress and egress, but we would expect these to correspond to the mid-points unless the light distribution is asymmetrical.) If a bright-spot eclipse is also present, care must be taken to ensure that, at this stage, the ingress and egress of the white

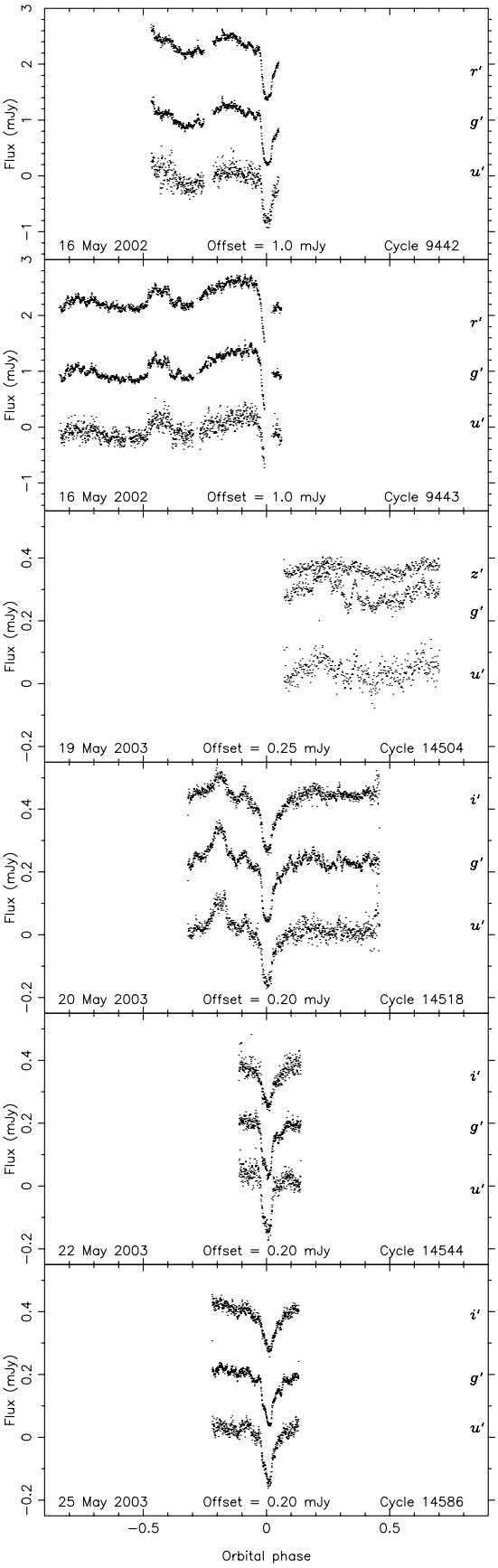

Figure 1. The light curve of OU Vir. The r', z' or i' data are offset vertically upwards and the u' data are offset vertically downwards.

Table 1. Mid-eclipse timings.

Date	HJD			
	u'	g'	r'	i'
2002 May 16	2 452 411.523 977	2 452 411.523 921	2 452 411.523 892	–
2003 May 20	2 452 780.580 157	2 452 780.580 278	–	2 452 780.580 217
2003 May 22	2 452 782.470 534	2 452 782.470 558	–	2 452 782.470 509
2003 May 25	2 452 785.524 083	2 452 785.524 083	–	2 452 785.524 255

Table 2. White dwarf contact phases and flux.

Date	Band	ϕ_{w1}	ϕ_{w2}	ϕ_{w3}	ϕ_{w4}	ϕ_{wi}	ϕ_{we}	Flux (mJy)
2002 May 16	u'	−0.024 414	−0.017 578	0.018 555	0.025 391	−0.020 508	0.022 461	–
	g'	−0.027 344	−0.018 555	0.016 602	0.025 391	−0.022 461	0.021 484	–
	r'	−0.028 320	−0.013 672	0.012 695	0.027 344	−0.020 508	0.020 508	–
2003 May 20	u'	−0.023 438	−0.016 602	0.018 555	0.025 491	−0.019 531	0.022 461	–
	g'	−0.025 391	−0.017 578	0.017 578	0.024 414	−0.021 484	0.021 484	–
	i'	−0.023 438	−0.014 648	0.016 602	0.025 391	−0.018 555	0.021 484	–
2003 May 22	u'	−0.024 414	−0.016 602	0.017 578	0.025 391	−0.020 508	0.021 484	–
	g'	−0.026 367	−0.018 555	0.016 602	0.024 414	−0.022 461	0.020 508	–
	i'	−0.021 484	−0.018 555	0.016 602	0.020 508	−0.019 531	0.018 555	–
2003 May 25	u'	−0.025 391	−0.016 602	0.014 648	0.023 438	−0.020 508	0.019 531	0.0537
	g'	−0.025 391	−0.019 531	0.016 602	0.022 461	−0.022 461	0.019 531	0.0519
	i'	−0.022 461	−0.018 555	0.017 578	0.022 461	−0.020 508	0.020 508	0.0146

dwarf are not confused with those of the bright spot. The eclipse contact phases corresponding to the start and the end of the ingress ϕ_1, ϕ_2 and the start and the end of the egress ϕ_3, ϕ_4 were determined by locating the points where the derivative differs significantly from a spline fit to the more slowly varying component.

Once the white dwarf eclipse contact phases have been found, the white dwarf light curve can be reconstructed and subtracted from the overall light curve, as illustrated in Fig. 2. The out-of-eclipse white dwarf fluxes thus found are given in Table 2. The white dwarf flux can be used to determine its temperature and distance (see Section 6). Once this has been done, the bright-spot eclipse contact phases (given in Table 3) can be determined by a similar method (Wood et al. 1989) and its light curve can be removed from that of the disc eclipse. If successful, this process can be used to determine the bright-spot temperature. Unfortunately, we were unsuccessful in our attempts to do this, probably because flickering hindered accurate determination of the bright-spot flux and contact phases.

In the discussion that follows, we use the suffixes 'w' and 'b' to denote white dwarf and bright-spot contact phases, respectively (e.g. ϕ_{wi} means the mid-ingress point of the white dwarf eclipse).

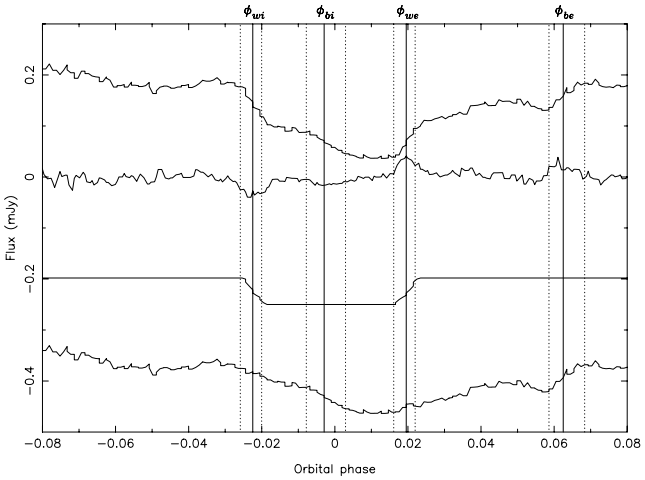

Figure 2. White dwarf deconvolution of the g' band light curve of 2003 May 25. From top to bottom: the data after smoothing by a median filter; the derivative after smoothing by a box-car filter and subtraction of the spline fit to this, multiplied by a factor of 5 for clarity; the reconstructed white dwarf light curve, shifted downwards by 0.25 mJy; the original light curve minus the white dwarf light curve after smoothing by a median filter, shifted downwards by 0.5 mJy. The vertical lines show the contact phases of the white dwarf and bright-spot eclipses, the dotted lines correspond to $\phi_{w1} \ldots \phi_{w4}$, $\phi_{b1} \ldots \phi_{b4}$ and the solid lines (labelled) correspond to ϕ_{wi}, ϕ_{we} and ϕ_{bi}, ϕ_{be}. The bright-spot ingress and egress are plainly visible, quickly following the white dwarf ingress and egress, respectively.

5 ORBITAL EPHEMERIS

A linear least-squares fit to the times of mid-eclipse given in Table 1 (calculated using the techniques described in Section 4 and taking the mid-point of the white dwarf eclipse as the point of mid-eclipse) and those of Vanmunster et al. (private communication) gives the following ephemeris:

$$\mathrm{HJD} = 2451725.03283 + 0.072706113\,E.$$
$$7\pm \qquad\qquad 5$$

Errors of $\pm 4 \times 10^{-5}$ d were used for the ULTRACAM data and errors of $\pm 7 \times 10^{-4}$ d were used for the Vanmunster et al. (private communication) data. This ephemeris was used to phase all of our data.

6 SYSTEM PARAMETERS

The derivation of the system parameters relies upon the fact that there is a unique relationship between the mass ratio and the orbital inclination for a given eclipse phase width $\Delta\phi = \phi_{we} - \phi_{wi}$, as follows.

Table 3. Bright-spot contact phases.

Date	Band	ϕ_{b1}	ϕ_{b2}	ϕ_{b3}	ϕ_{b4}	ϕ_{bi}	ϕ_{be}
2003 May 22	g'	−0.002 930	0.002 930	–	–	0.000 977	–
2003 May 25	u'	−0.007 813	0.002 930	0.060 547	0.065 430	−0.002 930	0.062 500
	g'	−0.007 813	0.002 930	0.058 594	0.068 359	−0.002 930	0.062 500

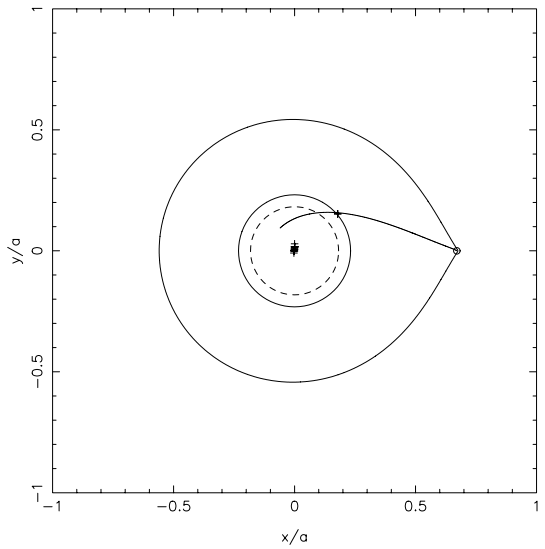

Figure 3. Trajectory of the gas stream from the secondary star for $q = 0.175$ and $i = 79.^{\circ}2$. Top: the system with the primary Roche lobe, L_1 point and disc of radius $R_d = 0.2315a$ plotted. The positions of the white dwarf and the bright-spot light centres corresponding to the observed ingress and egress phases for q and i as above are also plotted. The circularization radius (Verbunt 1988, equation 13) of $R_{circ} = 0.1820a$ is shown as a dashed circle. The stream passes through the bright-spot points (note that the timings of 2003 May 22 are of the ingress only, which prevents it from being plotted).

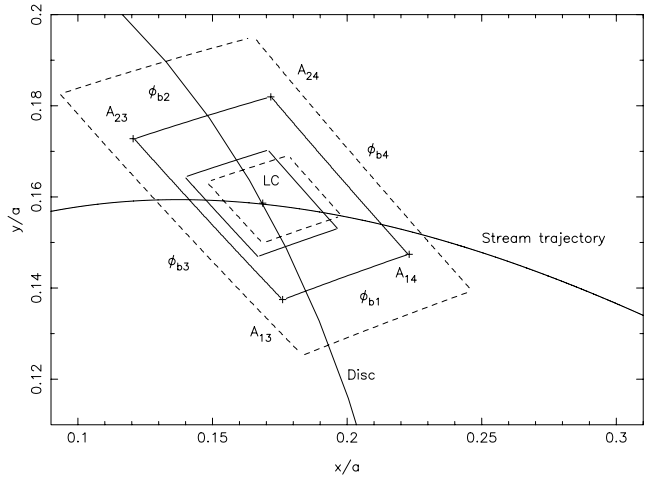

Figure 4. Horizontal structure of the bright spot for $q = 0.175$, showing the region on the orbital plane within which the bright spot lies. The light centre LC is marked by a cross, surrounded by the inner solid box which corresponds to the rms variations in position. The phase arcs which correspond to the bright-spot contact phases are shown as the outer solid box, with the rms variations in position shown as the two dashed boxes. Because all the timings of ϕ_{b2} and ϕ_{be} are identical, the rms variations of ϕ_{b1} and ϕ_{bi}, respectively, have been used instead. Intersections of the phase arcs ϕ_{bj} and ϕ_{bk} are marked A_{jk}, with crosses. The stream trajectory and disc of radius $R_d = 0.2315a$ are also plotted as solid curves.

(i) At smaller orbital inclinations, a larger secondary radius R_r is required in order to produce a given eclipse width.

(ii) The secondary radius is defined by the mass ratio because the secondary fills its Roche lobe.

(iii) Therefore, for a specific white dwarf eclipse width, the inclination is known as a function of the mass ratio.

The shape of the system does not depend on the orbital separation a; this just determines the scale. The orbital separation is determined by assuming a mass–radius relation for the primary (see later).

The trajectory of the gas stream originating from the inner Lagrangian point L_1 is calculated by solving the equations of motion (Flannery 1975) using a second-order Runge–Kutta technique and conserving the Jacobi energy to 1 part in 10^4. This assumes that the gas stream follows a ballistic path. Fig. 3 shows a theoretical gas stream for $q = 0.175$. Figs 4 and 5 show expanded views of the bright-spot region. As q decreases, the path of the stream moves away from the white dwarf. For a given mass ratio q, each point on the stream has a unique phase of ingress and egress.

For each phase, the limb of the secondary forms an arc when projected along the line of sight on to a given plane (hereafter referred to as a phase arc); each point on an individual phase arc is eclipsed at the same time. The intersection of the phase arcs corresponding to the respective eclipse contact phases can be used to constrain the size of the white dwarf and the structure of the bright spot. The light centres of the white dwarf and the bright spot must lie at the intersection of the phase arcs corresponding to the relevant phases of mid-ingress and mid-egress, ϕ_i and ϕ_e. The phase arcs were calculated using full Roche lobe geometry rather than an approximate calculation.

The mass ratio – and hence the inclination – may be determined by comparing the bright-spot light centres corresponding to the measured eclipse contact phases ϕ_{bi} and ϕ_{be} with the theoretical stream trajectories for different mass ratios q. This requires the assumption that the gas stream passes directly through the light centre of the bright spot. As illustrated in Figs 4 and 5, we constrain the light centre of the bright spot to be the point where the gas stream and the outer edge of the disc intersect, so that the distance from the primary at which the gas stream passes through the light centre of the bright spot gives the relative outer disc radius R_d/a.

The bright-spot timings thus yield a mass ratio of $q = 0.175 \pm 0.025$ and an inclination of $i = 79.^{\circ}2 \pm 0.^{\circ}7$ for an eclipse phase width $\Delta\phi = 0.041\,585$. The errors are determined by the rms variations in the measured contact phases. Figs 4 and 5 show the eclipse constraints on the structure of the bright spot. We use these to determine upper limits on the angular size and the radial and vertical extent of the bright spot, defining

$$\Delta\theta = (\theta_{23} + \theta_{24} - \theta_{13} - \theta_{14})/2 \quad (1)$$

$$\Delta R_d = (R_{24} + R_{14} - R_{23} - R_{13})/2 \quad (2)$$

$$\Delta Z = (H_{23} - H_{14})/2, \quad (3)$$

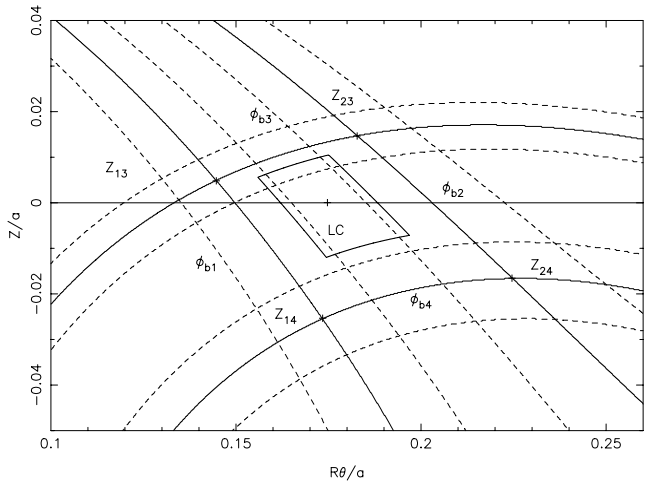

Figure 5. As Fig. 4, but showing the vertical structure of the bright spot. The phase arcs are projected on to a vertical cylinder of radius $0.2315a$ (equal to that of the disc), i.e. the x-axis is stepping around the edge of the disc. θ is in radians. The intersections of the phase arcs ϕ_{bj} and ϕ_{bk} are marked Z_{jk}, with crosses.

Table 4. Mean position and extent of the bright spot, as defined by equations (1)–(3). ΔZ_2 is calculated according to the definition used by Wood et al. (1986), for ease of comparison.

$\Delta R_d/a$	0.0417
$\Delta\theta$	15°.17
$\Delta Z/a$	0.0200
$\Delta Z_2/a$	0.0147
R_d/a	0.2315
θ	43°.24

where R_{jk} and θ_{jk} are the radius and azimuth of A_{jk}, and H_{jk} is the height of Z_{jk} above the orbital plane, as defined in Figs 4 and 5. θ increases in the direction of orbital motion and is zero at the line joining the centres of the two stars. Note that the definition of ΔZ in equation (3) differs slightly to that defined in Wood et al. (1986); this is in order to be more consistent with the definitions of $\Delta\theta$ and ΔR_d in equations (1) and (2). The mean position and extent of the bright spot are given in Table 4.

From Figs 4 and 5, we estimate that the gas stream passing through the light centre of the bright spot could just touch the phase arcs corresponding to ϕ_{b1} and ϕ_{b4} for a stream of circular cross-section with a radius $\varepsilon/a = 0.0175 \pm 0.0025$. The bright spot appears to be more extended azimuthally than radially, which can be understood by the shock front extending both up-disc and down-disc from the point of impact. The size of the stream is similar to that expected from theoretical studies (Lubow & Shu 1975, 1976) and that obtained by studies of similar objects (Wood et al. 1986, 1989), so our assumption that the stream passes through the light centre of the bright spot is reasonable.

Fig. 6 shows the eclipse constraints on the radius of the white dwarf. Using the mass ratio and orbital inclination derived earlier, we find that the white dwarf has a radius of $R_w = 0.013 \pm 0.004a$. An alternative possibility is that the sharp eclipse is caused by a bright inner disc region or boundary layer of radius $R_{belt} = 0.023 \pm 0.010a$ surrounding the white dwarf like a belt. These errors are

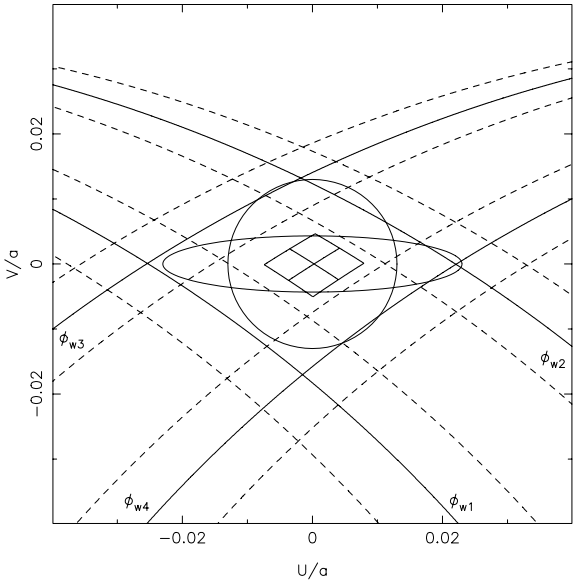

Figure 6. Projection of the white dwarf phase arcs on to the plane perpendicular to the line of sight. U and V are orthogonal coordinates perpendicular to the line of sight, U being parallel to the binary plane. Solid curves correspond to the contact phases of the white dwarf; dotted curves correspond to the rms variations of the phase arcs. The light centre is also plotted, surrounded by the solid box corresponding to the rms variations in phase. The projection of the white dwarf and accretion belt centred on U, $V = 0$ are shown for $R_w = 0.013a$ and $R_{belt} = 0.023a$.

calculated using the rms variations in the measured contact phases. Another possibility is that the lower hemisphere of the white dwarf is obscured by an optically thick accretion disc, which would result in the white dwarf radius being $R_w \geqslant 0.013a$. This is not the case, however, as the contact phases ϕ_{wi} and ϕ_{we} lie halfway through the white dwarf ingress and egress (see Section 4), i.e. the light centre in Fig. 6 lies at the origin and the light distribution is symmetrical.

The following analysis assumes that the eclipse is of a bare white dwarf. If the eclipse is actually of a belt and the white dwarf itself is not visible, then the white dwarf radius must be smaller than $R_{belt} = 0.023a$. If the white dwarf does contribute significantly to the eclipsed light, then we have the additional constraint that its radius must be $R_w \leqslant 0.013a$, so that the white dwarf mass given in Table 5 is actually a lower limit. The only way to verify the assumption that the central light source is the white dwarf alone is to measure the semi-amplitude of the radial velocity curve of the secondary star, K_r, and compare it to that predicted by the photometric model in Table 5. We could also check if this assumption is true using a longer baseline of quiescent observations, as one might expect eclipse timings of an accretion belt to be much more variable than those of a white dwarf. We note, however, that the white dwarf mass given in Table 5 is consistent with the mean white dwarf mass of $0.69 \pm 0.13\ M_\odot$ for CVs below the period gap (Smith & Dhillon 1998). Also, Baptista, Catalán & Costa (2000) point out that short-period dwarf novae (specifically OY Car, Z Cha and HT Cas) like OU Vir tend to accrete directly on to the white dwarf, whereas longer-period dwarf novae (IP Peg and EX Dra) usually have boundary layers. We will continue under the assumption that the central eclipsed object is indeed a bare white dwarf.

To determine the remaining system parameters, we have used the Nauenberg mass–radius relation for a cold, non-rotating white

Table 5. System parameters of OU Vir. The secondary radius given is the volume radius of the Roche lobe of the secondary (Eggleton 1983), as defined by equation (6). Parameters left blank in the right-hand column are independent of the model used.

Parameter	Nauenberg (cold)	Nauenberg (14 000 K)
Inclination i	$79\overset{\circ}{.}2 \pm 0\overset{\circ}{.}7$	
Mass ratio $q = M_{\rm r}/M_{\rm w}$	0.175 ± 0.025	
White dwarf mass $M_{\rm w}/{\rm M}_\odot$	0.85 ± 0.20	0.89 ± 0.20
Secondary mass $M_{\rm r}/{\rm M}_\odot$	0.15 ± 0.04	0.16 ± 0.04
White dwarf radius $R_{\rm w}/{\rm R}_\odot$	0.0095 ± 0.0030	0.0097 ± 0.0031
Secondary radius $R_{\rm r}/{\rm R}_\odot$	0.177 ± 0.024	0.180 ± 0.024
Separation $a/{\rm R}_\odot$	0.73 ± 0.06	0.74 ± 0.05
White dwarf radial velocity $K_{\rm w}/{\rm km\ s^{-1}}$	75 ± 12	76 ± 12
Secondary radial velocity $K_{\rm r}/{\rm km\ s^{-1}}$	426 ± 6	432 ± 6
Outer disc radius $R_{\rm d}/a$	0.2315 ± 0.0150	
Distance D/pc	51 ± 17	
White dwarf temperature $T_{\rm w}$/K	$13\,900 \pm 600$	

dwarf (Nauenberg 1972; Cook & Warner 1984),

$$R_{\rm w} = 7.795 \times 10^6 \left[\left(\frac{1.44\,{\rm M}_\odot}{M_{\rm w}} \right)^{2/3} - \left(\frac{M_{\rm w}}{1.44\,{\rm M}_\odot} \right)^{2/3} \right]^{1/2} {\rm m}, \tag{4}$$

which gives an analytical approximation to the Hamada–Salpeter mass–radius relation (Hamada & Salpeter 1961). If we set $R_{\rm w}/a = y$, we can rewrite Kepler's third law in terms of the parameters $R_{\rm w}$ and y, giving another restriction on the white dwarf radius:

$$R_{\rm w} = y \left[\frac{G M_{\rm w} (1+q) P^2}{4\pi^2} \right]^{1/3}. \tag{5}$$

Equations (4) and (5) can be easily solved to give the system parameters, given in Table 5. The secondary radius $R_{\rm r}$ has been calculated by approximating it to the effective radius of the Roche lobe (Eggleton 1983):

$$R_{\rm L} = \frac{0.49 a q^{2/3}}{0.6 q^{2/3} + \ln(1 + q^{1/3})}, \quad 0 < q < \infty, \tag{6}$$

which is accurate to better than 1 per cent. Because the Nauenberg (1972) mass–radius relation assumes a cold white dwarf, we have attempted to correct this relation to a temperature of ∼14 000 K, the approximate temperature given by the blackbody fit below. Wood et al. (1989) and Koester & Schönberner (1986) note that the radius of a white dwarf at 10 000 K is about 5 per cent larger than a cold white dwarf. To correct from 10 000 to 14 000 K, we have used the white dwarf cooling curves of Wood (1995), which gives a total radial correction of 6.2 per cent. This alternative model is also given in Table 5 and is quoted for all temperature-dependent parameters.

The expected flux from a blackbody $B_\nu(\lambda, T)$ in a passband with transmission function $P(\lambda)$ is (e.g. Wood et al. 1989)

$$f = \frac{\int P(\lambda) B_\nu(\lambda, T)\, {\rm d}\lambda/\lambda}{\int P(\lambda)\, {\rm d}\lambda/\lambda} \frac{\pi R_{\rm w}^2}{D^2}, \tag{7}$$

where D is the distance to the star. By fitting a blackbody function to the white dwarf flux in each passband, given in Table 2, we derive a white dwarf temperature of $T_{\rm w} = 13\,900 \pm 600$ K and $D = 51 \pm 17$ pc (assuming $R_{\rm w} = 0.0097 \pm 0.0031\ {\rm R}_\odot$). We would expect some systematic errors to be present in these estimates as we have only used one eclipse and not an averaged light curve, so flickering is likely to be a problem.

7 CONCLUSIONS

We have presented an analysis of five eclipses of OU Vir, some in superoutburst and some in quiescence. The quiescent eclipses have been used to make the first determination of the system parameters, given in Table 5. Our main conclusions are as follows.

(i) Eclipses of both the white dwarf and the bright spot were observed during quiescence. The identification of the bright-spot ingress and egress appears to be unambiguous.

(ii) By requiring the gas stream to pass directly through the light centre of the bright spot, the mass ratio and orbital inclination were found to be $q = 0.175 \pm 0.025$ and $i = 79\overset{\circ}{.}2 \pm 0\overset{\circ}{.}7$.

(iii) Assuming that the central eclipsed object is circular, that its size accurately reflects that of the white dwarf and that it obeys the Nauenberg (1972) approximation to the Hamada & Salpeter (1961) mass–radius relationship, adjusted to $T = 14\,000$ K, we find that the white dwarf radius is $R_{\rm w} = 0.0097 \pm 0.0031\ {\rm R}_\odot$ and that its mass is $M_{\rm w} = 0.89 \pm 0.20\ {\rm M}_\odot$.

(iv) With the same assumptions, we find that the volume radius of the secondary star is $R_{\rm r} = 0.180 \pm 0.024\ {\rm R}_\odot$ and that its mass is $M_{\rm r} = 0.16 \pm 0.04\ {\rm M}_\odot$. The secondary star is therefore consistent with the empirical mass–radius relation for the main-sequence secondary stars in CVs of Smith & Dhillon (1998).

(v) A blackbody fit to the white dwarf flux gives a temperature $T_{\rm w} = 13\,900 \pm 600$ K and a distance $D = 51 \pm 17$ pc with the same assumptions as above. These are purely formal errors from the least-squares fit using estimated errors of ±0.01 mJy for each flux measurement. Given that we use data from only one eclipse, with a single measurement of the flux from each passband, the actual uncertainties are likely to be significantly larger.

(vi) The accretion disc radius of $R_{\rm d}/a = 0.2315 \pm 0.0150$ is similar in size to that of HT Cas, for which Horne, Wood & Steining (1991) derived $R_{\rm d}/a = 0.23 \pm 0.03$. This is small compared to many other dwarf novae (e.g. Z Cha, which has $R_{\rm d}/a = 0.334$; Wood et al. 1989), but larger than the circularization radius (Verbunt 1988, equation 13) of $R_{\rm circ} = 0.1820a$. We note that this is an unusually small disc radius. It is especially surprising because this disc radius was determined from observations obtained only 20 days after the superoutburst was first reported (Kato 2003).

(vii) The superhump period of OU Vir is $P_{\rm sh} = 0.078 \pm 0.002$d (Vanmunster et al. 2000), which means that OU Vir lies 5σ off the superhump period excess–mass ratio relation of Patterson (1998 equation 8), with the superhump period excess $\epsilon = (P_{\rm sh} - P_{\rm orb})/P_{\rm orb}$

~ 0.073. However, it does not lie on the superhump period excess–orbital period relation either, perhaps indicating that the current estimate of the superhump period $P_{\rm sh}$ is inaccurate.

ACKNOWLEDGMENTS

We thank the anonymous referee for useful comments. We are grateful to Tonny Vanmunster for providing his times of mid-eclipse. WJF would like to thank Timothy Thoroughgood for helpful discussions. WJF, MJS and CSB are supported by PPARC studentships. CAW is employed on PPARC grant PPA/G/S/2000/00598. ULTRACAM is funded by PPARC grant PPA/G/S/2002/00092.

REFERENCES

Baptista R., Catalán M. S., Costa L., 2000, MNRAS, 316, 529
Cook M. C., Warner B., 1984, MNRAS, 207, 705
Dhillon V. S., Marsh T. R., 2001, New Astron. Rev., 45, 91
Eggleton P. P., 1983, ApJ, 268, 368
Flannery B. P., 1975, MNRAS, 170, 325
Fukugita M., Ichikawa T., Gunn J. E., Doi M., Shimasaku K., Schneider D. P., 1996, AJ, 111, 1748
Hamada T., Salpeter E. E., 1961, ApJ, 134, 683
Horne K., Wood J. H., Steining R. F., 1991, ApJ, 378, 271
Kato T., 2003, vsnet-alert, No. 7733 http://vsnet.kusastro.kyoto-u.ac.jp/vsnet/index.html
King D. L., 1985, RGO/La Palma Technical Note 31, Atmospheric Extinction at the Roque de los Muchachos Observatory, La Palma
Koester D., Schönberner D., 1986, A&A, 154, 125
Lubow S. H., Shu F. H., 1975, ApJ, 198, 383
Lubow S. H., Shu F. H., 1976, ApJ, 207, L53
Mason E., Howell S. B., Szkody P., Harrison T. E., Holtzman J. A., Hoard D. W., 2002, A&A, 396, 633
Nauenberg M., 1972, ApJ, 175, 417
Patterson J., 1998, PASP, 110, 1132
Rutten R. G. M., Kuulkers E., Vogt N., van Paradijs J., 1992, A&A, 265, 159
Smith D. A., Dhillon V. S., 1998, MNRAS, 301, 767
Smith J. A. et al., 2002, AJ, 123, 2121
Vanmunster T., Velthuis F., McCormick J., 2000, Inf. Bull. Variable Stars, 4955
Verbunt F., 1988, ApJ, 332, 193
Wood J. H., Irwin M. J., Pringle J. E., 1985, MNRAS, 214, 475
Wood J. H., Horne K., Berriman G., Wade R., O'Donoghue D., Warner B., 1986, MNRAS, 219, 629
Wood J. H., Horne K., Berriman G., Wade R., 1989, ApJ, 314, 974
Wood M. A., 1995, in Koester D., Werner K., eds, Lect. Notes Phys., Vol. 443, European Workshop on White Dwarfs. Springer-Verlag, Berlin, p. 41

This paper has been typeset from a TEX/LATEX file prepared by the author.